

# RIS-aided OTFS with Index Modulation

Vighnesh S Bhat and A. Chockalingam

Department of ECE, Indian Institute of Science, Bangalore 560012

**Abstract**—Reconfigurable intelligent surfaces (RIS) technology, orthogonal time frequency space (OTFS) modulation, and index modulation (IM) are promising physical layer techniques in wireless communications. An RIS system steers the electromagnetic wave towards the receiver using an electronically tunable surface. OTFS delivers robust performance in high mobility scenarios using information signalling in the delay-Doppler (DD) domain, and IM can offer improved spectral efficiencies and bit error performance. In this paper, we propose an RIS-aided OTFS scheme in which IM is carried out in the DD domain. We call the proposed scheme as RIS-aided OTFS-IM scheme. We develop an end-to-end DD domain input-output relation for the proposed RIS-aided OTFS-IM scheme and evaluate its bit error performance. Our results show that 1) the performance of RIS-aided OTFS improves significantly with the proposed DD domain indexing and increased number of RIS elements, 2) among the phase selection schemes considered at the RIS, Frobenius norm based phase selection achieves superior performance, and 3) RIS-aided OTFS-IM performs better than RIS-aided OFDM-IM.

**Index Terms**—Reconfigurable intelligent surface, OTFS modulation, index modulation, delay-Doppler domain, RIS-aided OTFS-IM.

## I. INTRODUCTION

In the rapidly evolving world of next-generation wireless technologies such as 6G, the air interface and the modulation waveform must be capable of meeting challenging performance and system requirements in terms of robustness in high-Doppler wireless environments, high reliability, increased power/spectral efficiencies, and low latency. To meet these requirements, several new physical layer techniques have emerged. They include reconfigurable intelligent surfaces (RIS) [1]- [4], orthogonal time-frequency space (OTFS) modulation [5]- [7], and index modulation (IM) [8]- [10]. RIS technology provides energy-efficient wireless communication, OTFS modulation provides reliable high-mobility support, and IM technique offers improved spectral efficiency and performance.

An RIS assisted communication system uses low-cost, passively tunable reflecting elements to aid communication between transmitter and receiver. The reflector phases are tuned to steer the incident signal towards the receiver to achieve a significant increase in the received signal-to-noise ratio. Since the RIS elements do not require extra energy to process incident radio frequency (RF) signals, this technique is energy-efficient. OTFS modulation has gained attention for its robustness in high-Doppler channels [5]. It is more robust than other multicarrier modulation schemes such as orthogonal frequency division multiplexing (OFDM) [6], [7]. In high-mobility environments, the channel changes rapidly in time. As

a result, the performance of OFDM is degraded due to inter-carrier interference. OTFS modulation tackles these limitations by multiplexing the information symbols in the delay-Doppler (DD) domain instead of the time-frequency (TF) domain that OFDM uses. In IM, information bits are conveyed through indexing of transmission entities like transmit antennas, time slots, etc. IM offers performance, RF hardware complexity, and spectral efficiency benefits [10]. Following this trend, IM concept has been explored in multicarrier modulation, such as OFDM [11] and OTFS [12]- [15], where subcarrier and DD bin indices are used to convey information bits.

Owing to their inherent strengths and the benefits they can offer, research in RIS, OTFS, and IM have been growing. Recent works have started investigating systems that exploit the strengths of combinations of these techniques [12]- [18]. Some recent works have investigated OTFS with IM and demonstrated the performance gains achieved through indexing of DD bins in OTFS [12]- [15]. The work in [12] showed that OTFS with indexing can outperform OFDM with indexing. The work in [13] showed that the diversity and peak-to-average power ratio (PAPR) of OTFS are improved using indexing. In [14], a dual mode indexing scheme in OTFS and a minimum Hamming distance based log-likelihood ratio detector are reported. In [15], an enhanced IM scheme in OTFS that exploited the in-phase and quadrature dimensions for improved spectral efficiency is reported. Some recent works have investigated OTFS systems that are aided by RIS [16]- [18]. RIS-aided OTFS systems have been investigated in [16], [17], where end-to-end input-output relation in the DD domain has been derived and the bit error performance evaluated in high-mobility environments. MIMO-OTFS system aided by RIS has been studied in [18]. The performance gains achieved using RIS in OTFS systems are illustrated in these works.

We note that a combination of RIS, OTFS, and IM can offer the simultaneous benefits of energy efficiency (due to RIS), robustness against Doppler (due to OTFS), and spectral efficiency (due to IM). To our knowledge, an investigation of RIS-aided OTFS with IM has not been reported. Therefore, in this paper, we investigate an RIS-aided OTFS scheme with IM, where IM is carried out in the DD domain (see Table I). We call the proposed scheme as RIS-aided OTFS-IM scheme. We develop an end-to-end end-to-end DD domain input-output relation for the proposed RIS-aided OTFS-IM scheme, and evaluate its bit error performance. Our simulation results show that 1) the performance of RIS-aided OTFS improves with DD domain indexing and increase in the number of RIS elements, 2) among the phase selection schemes considered at the RIS, Frobenius norm based phase selection achieves superior performance, and 3) the proposed RIS-aided OTFS-

Reference	RIS	OTFS	DD domain IM
[12], [13], [14], [15]	×	✓	✓
[16], [17], [18]	✓	✓	×
Proposed scheme	✓	✓	✓

TABLE I: Summary of literature survey.

IM performs better than RIS-aided OFDM-IM.

The remainder of the paper is organized as follows. The system model of the proposed RIS-aided OTFS-IM scheme is developed in Sec. II. The RIS phase selection is discussed in Sec. III. Results and discussions are presented in Sec. IV. Conclusions and possible future work are presented in Sec. V.

*Notations:* A vector is represented by a boldface lower case letter and matrix by a boldface upper case letter.  $\lfloor \cdot \rfloor$ ,  $[\cdot]_N$ , and  $|\cdot|$  represent the floor function, modulo- $N$  operation, and absolute value of a number, respectively. The Frobenius norm of matrix is denoted by  $\|\cdot\|$ , angle of a complex number by  $\angle \cdot$ , and set of all complex numbers by  $\mathbb{C}$ .

## II. RIS-AIDED OTFS-IM SYSTEM MODEL

The proposed RIS-aided OTFS system with IM in the DD domain is presented in this section. In this scheme, information bits are carried by 1) complex symbols from a modulation alphabet multiplexed in the DD grid, and 2) indexing of the DD bins in the DD grid. The DD grid is of size  $M \times N$ , where  $M$  and  $N$  are the number of delay and Doppler bins, respectively, and  $MN$  is the number of DD bins in the grid, which constitutes one OTFS frame.

### A. DD indexing in OTFS

For the purpose of indexing, the DD grid is partitioned into multiple sub-blocks, each sub-block (SB) having multiple DD bins. Indexing is done across the DD bins in each SB. Let  $C$  denote the number of SBs and  $u$  denote the number of DD bins per SB. Then,

$$C = \frac{MN}{u}.$$

Indexing in an SB is done in such a way that  $v$  DD bins among the  $u$  DD bins in a SB are made active and the remaining  $u-v$  DD bins are left idle. Each active bin in an SB is loaded with a complex symbol from a modulation alphabet  $\mathbb{A}$  and the idle bins are loaded with zero. Therefore, the number of index bits per SB, denoted by  $b_1$ , is given by  $b_1 = \lfloor \log_2 \binom{u}{v} \rfloor$ , and the total number of index bits in the entire DD grid is given by  $Cb_1 = C \lfloor \log_2 \binom{u}{v} \rfloor$ .

Since there are  $v$  active DD bins in an SB, the number of modulation bits per SB, denoted by  $b_2$ , is given by  $b_2 = v \log_2 |\mathbb{A}|$ , where  $|\mathbb{A}|$  is the size of the modulation alphabet  $\mathbb{A}$ . So, the total number of modulation bits in the entire grid is given by  $Cb_2 = Cv \log_2 |\mathbb{A}|$ . The total number of index bits and modulation bits per SB, denoted by  $b$ , is given by  $b = b_1 + b_2$ , and the total number index bits and modulation bits in the entire DD grid (i.e., total number of bits per OTFS frame) is therefore given by

$$Cb = C(b_1 + b_2) = C \left[ \lfloor \log_2 \binom{u}{v} \rfloor + v \log_2 |\mathbb{A}| \right].$$

$b_1$ index bits	Indices of active DD bins in an SB
00	(1, 2, 3)
01	(2, 3, 4)
10	(3, 4, 1)
11	(1, 2, 4)

TABLE II: An example mapping of index bits to DD bin indices in an SB for  $u = 4$ ,  $v = 3$ ,  $b_1 = 2$ .

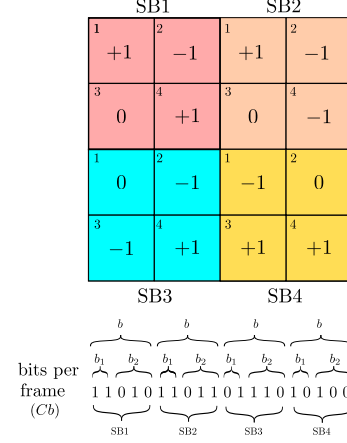


Fig. 1: Illustration of DD domain indexing for  $M = N = 4$ ,  $u = 4$ ,  $v = 3$ , and BPSK modulation.

Therefore, the achieved rate of OTFS with the above IM, in bits per channel use (bpcu), is given by

$$\eta = \frac{C}{MN} \left[ \lfloor \log_2 \binom{u}{v} \rfloor + v \log_2 |\mathbb{A}| \right]. \quad (1)$$

*Example:* To illustrate the above IM scheme, consider  $M = N = 4$ ,  $u = 4$ ,  $v = 3$ , and BPSK modulation. Here,  $C = \frac{MN}{u} = \frac{16}{4} = 4$ ,  $b_1 = \lfloor \log_2 \binom{u}{v} \rfloor = \lfloor \log_2 \binom{4}{3} \rfloor = 2$ ,  $b_2 = v \log_2 |\mathbb{A}| = 3 \log_2 2 = 3$ ,  $b = b_1 + b_2 = 5$ , and  $\eta = 1.25$  bpcu. A mapping of index bits to DD bin indices in an SB for this example is shown in Table II. Considering the mapping in Table II, Fig. 1 shows the DD grid with active bins loaded with BPSK symbols ( $0 \rightarrow +1$  and  $1 \rightarrow -1$ ) and idle bins loaded with zeros for the  $Cb = 20$ -length information bit sequence 11010 11011 01110 10100. The  $MN = 16$  symbols in the DD grid shown in Fig. 1 are fed as input to the OTFS modulator. Note that if indexing is not performed in the considered example, then the achieved rate is 1 bpcu, whereas the achieved rate is 1.25 bpcu with DD indexing.

### B. RIS-aided OTFS-IM system

The proposed RIS-aided OTFS-IM system is shown in Fig. 2. The transmitter consists of the IM encoder (as described in the previous subsection), followed by the OTFS modulator. The transmitter is aided by an RIS having multiple reflecting elements. A sub-surface that has a common reflection coefficient is formed by combining adjacent elements with highly correlated channel gains [4]. Accordingly, the RIS consists of  $L$  reflecting elements, grouped into  $S$  sub-surfaces, each with

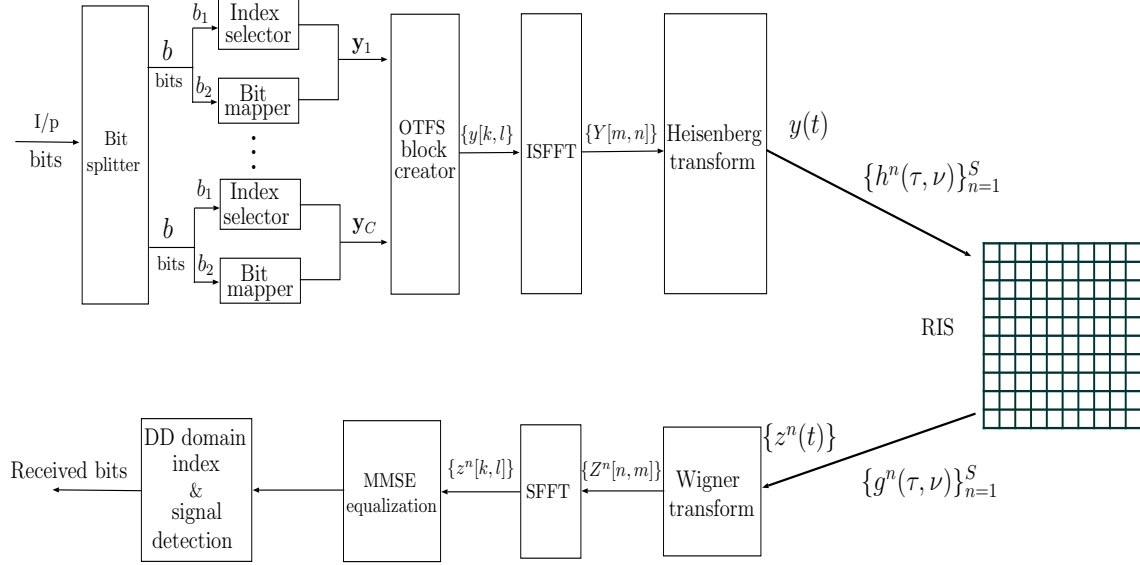


Fig. 2: RIS-aided OTFS with index modulation.

$N_s = L/S$  adjacent reflecting elements. Let  $\theta_n = \alpha_n e^{j\phi_n}$ , be the reflection coefficient of the  $n$ th sub-surface with  $\alpha_n \in [0, 1]$  being the amplitude and  $\phi_n \in [-\pi, \pi]$  being the phase of the  $n$ th sub-surface.

In the IM scheme (described in the previous subsection), the entries of the  $j$ th SB can be written as

$$\mathbf{y}_j = [y_{j,1}, y_{j,1}, \dots, y_{j,u}], \quad 1 \leq j \leq C, \quad (2)$$

where  $y_{j,i} \in \mathbb{A} \cup \{0\}$ . The OTFS block creator combines all the SBs and generates the DD domain symbols  $y[k, l]$ ,  $0 \leq k \leq N-1$ ,  $0 \leq l \leq M-1$  as input to the OTFS modulator. The OTFS modulation scheme uses a bandwidth of  $M\Delta f$  and a frame duration of  $NT$  with  $\Delta f = \frac{1}{T}$ . The OTFS modulator converts the DD domain symbols to TF symbols using inverse symplectic fourier transform (ISFFT). These TF domain symbols are then converted to time domain using Heisenberg transform for transmission. The TF domain signal  $Y[m, n]$  after ISFFT is given by

$$Y[n, m] = \frac{1}{\sqrt{MN}} \sum_{k=0}^{N-1} \sum_{l=0}^{M-1} y[k, l] e^{j2\pi(\frac{nk}{N} - \frac{ml}{M})}. \quad (3)$$

Using Heisenberg transform, the TF signal  $Y[m, n]$  is converted to time domain signal  $y(t)$ , given by

$$y(t) = \sum_{n=0}^{N-1} \sum_{m=0}^{M-1} Y[n, m] p_{tx}(t - nT) e^{j2\pi m \Delta f (t - nT)}, \quad (4)$$

where  $p_{tx}(t)$  is the transmit pulse. The time domain signal  $y(t)$  is then transmitted through the time-varying wireless channel of the first link (i.e., transmitter-to-RIS link). The DD response of the channel between the transmitter and the  $n$ th sub-surface of the RIS is given by

$$h^n(\tau, \nu) = \sum_{p=1}^{P_1} h_p^n \delta(\tau - \tau_p^{n,1}) \delta(\nu - \nu_p^{n,1}), \quad (5)$$

where  $P_1$  is the number of paths in the first link,  $h_p^n$ ,  $\tau_p^{n,1}$ , and  $\nu_p^{n,1}$  denote the fade coefficient, delay, and Doppler, respectively, of the  $p$ th path in the first link associated with the  $n$ th sub-surface. At the  $n$ th sub-surface of the RIS, the signal received is given by

$$w^n(t) = \int_{\nu} \int_{\tau} h^n(\tau, \nu) y(t - \tau) e^{j2\pi\nu(t - \tau)} d\tau d\nu. \quad (6)$$

The signal  $w^n(t)$  then goes through the second link (i.e., RIS-to-receiver link). The DD channel response between the  $n$ th sub-surface of the RIS and the receiver is given by

$$g^n(\tau, \nu) = \sum_{q=1}^{P_2} g_q^n \delta(\tau - \tau_q^{n,2}) \delta(\nu - \nu_q^{n,2}), \quad (7)$$

where  $P_2$  is the number of paths in the second link,  $g_q^n$ ,  $\tau_q^{n,2}$ , and  $\nu_q^{n,2}$  denote the fade coefficient, delay, and Doppler, respectively, of the  $q$ th path in the second link associated with the  $n$ th sub-surface. The delay and Doppler of the  $p$ th path in the first link and  $q$ th path in the second link can be written as

$$\tau_p^{n,1} \triangleq \frac{\gamma_p^{n,1}}{M\Delta f}, \quad \nu_p^{n,1} \triangleq \frac{\delta_p^{n,1}}{NT}, \quad \tau_q^{n,2} \triangleq \frac{\gamma_q^{n,2}}{M\Delta f}, \quad \nu_q^{n,2} \triangleq \frac{\delta_q^{n,2}}{NT}, \quad (8)$$

where  $\gamma_p^{n,1}$ ,  $\delta_p^{n,1}$ ,  $\gamma_q^{n,2}$ ,  $\delta_q^{n,2}$  are assumed to be integers. The received signal reflected from the  $n$ th sub-surface is given by

$$\begin{aligned} z^n(t) &= \theta_n \int_{\nu_2} \int_{\tau_2} g^n(\tau_2, \nu_2) w^n(t - \tau_2) e^{j2\pi\nu_2(t - \tau_2)} d\tau_2 d\nu_2 \\ &= \theta_n \int_{\nu_2} \int_{\tau_2} g^n(\tau_2, \nu_2) \left[ \int_{\nu_1} \int_{\tau_1} h^n(\tau_1, \nu_1) y(t - \tau_1 - \tau_2) \right. \\ &\quad \left. e^{j2\pi\nu_1(t - \tau_1 - \tau_2)} d\tau_1 d\nu_1 \right] e^{j2\pi\nu_2(t - \tau_2)} d\tau_2 d\nu_2. \end{aligned} \quad (9)$$

Matched filtering is carried out at the receiver using Wigner transform to get the TF domain signal  $Z^n[n, m]$  as

$$Z^n[n, m] = Z^n(t, f)|_{t=nT, f=m\Delta f}, \quad (10)$$

where  $Z^n(t, f)$  is the cross-ambiguity function between the received signal  $z^n(t)$  and the receive pulse  $p_{rx}(t)$ , given by

$$Z^n(t, f) = \int_{t'} p_{rx}^*(t' - t) z^n(t') e^{-j2\pi f(t' - t)} dt'. \quad (11)$$

The TF domain signal is transformed to DD domain using symplectic finite fourier transform (SFFT) as

$$z^n[k, l] = \frac{1}{\sqrt{MN}} \sum_{n=0}^{N-1} \sum_{m=0}^{M-1} Z^n[n, m] e^{-j2\pi(\frac{nk}{N} - \frac{ml}{M})}. \quad (12)$$

Assuming that the pulses  $p_{tx}(t)$  and  $p_{rx}(t)$  satisfy bi-orthogonal condition, the end-to-end DD domain input-output relation associated with the  $n$ th sub-surface can be written as [16]

$$z^n[k, l] = \theta_n \sum_{q=1}^{P_2} g_q^n e^{-j2\pi\nu_q^{n,2}\tau_q^{n,2}} \sum_{p=1}^{P_1} h_p^n e^{-j2\pi\nu_p^{n,1}(\tau_p^{n,1} + \tau_q^{n,2})} y[[k - (\delta_p^{n,1} + \delta_q^{n,2})]_N, [l - (\gamma_p^{n,1} + \gamma_q^{n,2})]_M]. \quad (13)$$

Vectorizing the expression in (13), we get

$$\mathbf{z}^n = \theta_n \mathbf{G}^n \mathbf{y}, \quad (14)$$

where  $\mathbf{z}^n, \mathbf{y} \in \mathbb{C}^{MN \times 1}$ . The  $(k + Nl)$ th entry of  $\mathbf{y}$  is  $y_{k+Nl} = y[k, l]$ , for  $k = 0, \dots, N-1, l = 0, \dots, M-1$  and  $y[k, l] \in \mathbb{A} \cup \{0\}$ . In a similar way, the  $(k + Nl)$ th entry of  $\mathbf{z}^n$  is  $z_{k+Nl}^n = z^n[k, l]$ , for  $k = 0, \dots, N-1, l = 0, \dots, M-1$ , and  $\mathbf{G}^n \in \mathbb{C}^{MN \times MN}$  is the overall cascaded channel matrix for the  $n$ th sub-surface. The overall end-to-end DD domain signal is obtained by combining the reflected signals from the all the  $S$  sub-surfaces. Therefore, the end-to-end input-output relation in vector form is given by

$$\mathbf{z} = \sum_{n=1}^S \theta_n \mathbf{G}^n \mathbf{y} + \mathbf{u}, \quad (15)$$

where  $\mathbf{z}$  is the sum of all the received vectors from all the sub-surfaces and  $\mathbf{u} \in \mathbb{C}^{MN \times 1}$  is the receiver noise vector.

### C. Detection

For small-sized frames (i.e., small values of  $M, N$ ), maximum likelihood (ML) detection can be used. However, for large frames, ML detection is prohibitively complex. Instead, minimum mean square error (MMSE) detection can be used. At the receiver, after Wigner transform and SFFT, MMSE equalization is performed to get  $\hat{\mathbf{y}}$ . ML detection is then used on each SB to search all possible index combinations and modulated symbols jointly.

### III. REFLECTION PHASE DESIGN

The design of the RIS reflection phases focuses on the maximization of signal power at the receiver. The main advantage of RIS is its ability to tune the reflection phases depending on the channel conditions. Without loss of generality, we take  $\alpha_n = 1, n = 1, \dots, S$ , and consider three different schemes to obtain  $\phi_n, n = 1, \dots, S$  at the RIS.

1) *Blind phase*: In this scheme, the phase  $\phi_n$  is selected to be zero, i.e.,  $\phi_n = 0, n = 1, \dots, S$ . Though this scheme

Path	1	2	3	4	5
Delay ( $\tau_j$ ), $\mu\text{s}$	2.08	4.164	6.246	8.328	10.41
Doppler ( $\nu_j$ ), Hz	0	470	940	1410	1880

TABLE III: DD profile for  $P_1 = P_2 = 5$ .

does not utilize the beamforming feature of RIS, it serves as a scheme for comparison.

*Frobenius norm-based phase*: In this method of phase selection, the phases at the RIS are chosen so as to maximize the Frobenius norm of the end-to-end channel matrix. Let the reflection phase vector be  $\Phi = [\phi_1, \phi_2, \dots, \phi_S]$ . We are interested in the maximization of  $\|\sum_{n=1}^S e^{j\phi_n} \mathbf{G}^n\|^2$ . The approximate solution to the maximization problem can be obtained by using random Monte Carlo sampling. Let  $\Phi^i = [\phi_1^i, \phi_2^i, \dots, \phi_S^i]$  be the  $i$ th realization of the phase vector. A large number of such vectors are generated, and that vector is chosen which maximizes the quantity  $\|\sum_{n=1}^S e^{j\phi_n} \mathbf{G}^n\|^2$ .

*Strongest DD channel response phase (DDRC)*: This method selects the RIS phase in such a way that the strongest DD channel aligns with the direct beam. A simple exhaustive search among the  $P_1 P_2$  path pairs is carried out to identify the strongest  $(h_p^n, g_q^n)$  pair. The above problem can be formulated as [18]

$$(\hat{p}, \hat{q}) = \arg \max_{p, q} |h_p^n g_q^n|. \quad (16)$$

The phase for the  $n$ th sub-surface is given by

$$\phi_n = -\angle h_{\hat{p}}^n g_{\hat{q}}^n. \quad (17)$$

The phase of the  $n$ th sub-surface is therefore opposite to the phase of the strongest cascaded transmit-RIS-receive path.

### IV. RESULTS AND DISCUSSIONS

This section presents the simulated bit error rate (BER) performance of the proposed RIS-aided OTFS-IM scheme. The following parameters are considered in the simulations: ( $M = 4, N = 2$ ) with  $u = 8, v = 6$ , ( $M = N = 16$ ) with  $u = 4, v = 3$ , and 4-QAM. A subcarrier spacing of  $\Delta f = 3.75$  kHz and a carrier frequency of  $f_c = 4$  GHz is considered. For the first link in the ( $M = 4, N = 2$ ) system,  $P_1 = 2$  paths with DD profile of  $(\tau_i, \nu_i) = [(0, 0), (1/(M\Delta f), 1/(NT))]$  is considered. For the second link,  $P_2 = 2$  with DD profile of  $(\tau_i, \nu_i) = [(0, 0), (1/(M\Delta f), 0)]$  is considered. For the ( $M = N = 16$ ) system,  $P_1 = P_2 = 5$  with the DD profile in Table III is used. For both links, the fade coefficients are assumed to be i.i.d complex Gaussian with zero mean and variance of  $1/P$ , where  $P$  represents the number of paths. Perfect channel knowledge at the receiver is assumed.

*Performance of RIS-aided OTFS without and with indexing*: Figure 3 shows the BER performance of RIS-aided OTFS with and without indexing for  $S = 4, 8, M = 4, N = 2, u = 8, v = 6, P_1 = P_2 = 2$ , Frobenius norm based phase selection, and ML detection. From Fig. 3, it is observed that the performance of RIS-aided OTFS improves with indexing. For  $S = 4$ , at a BER of  $10^{-5}$ , there is an SNR advantage of about 5 dB in favor of RIS-aided OTFS with indexing. Also, as the number of sub-surfaces increases ( $S = 8$ ), the performance improves.

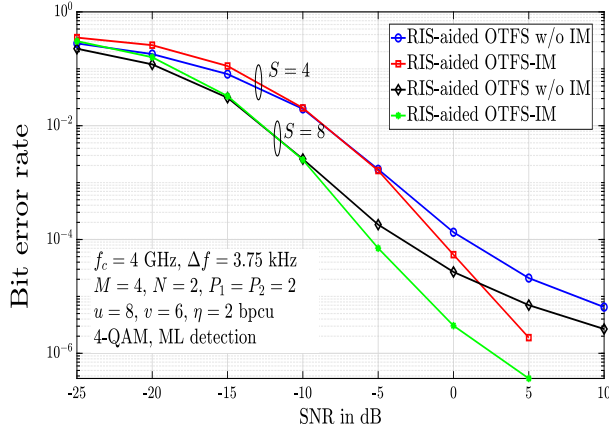


Fig. 3: BER performance of RIS-aided OTFS without and with indexing.

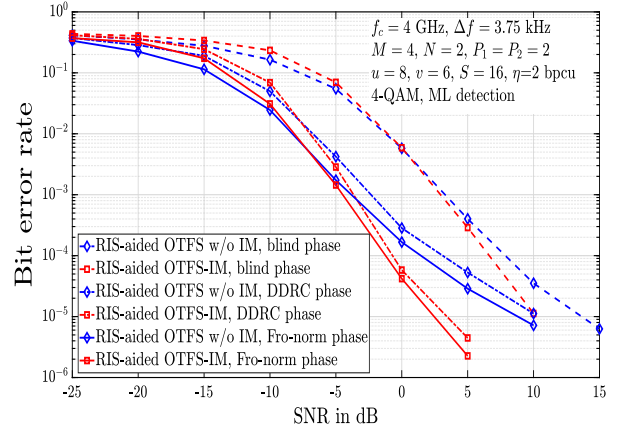


Fig. 5: Performance of RIS-aided OTFS without and with indexing for different types of phase selection.

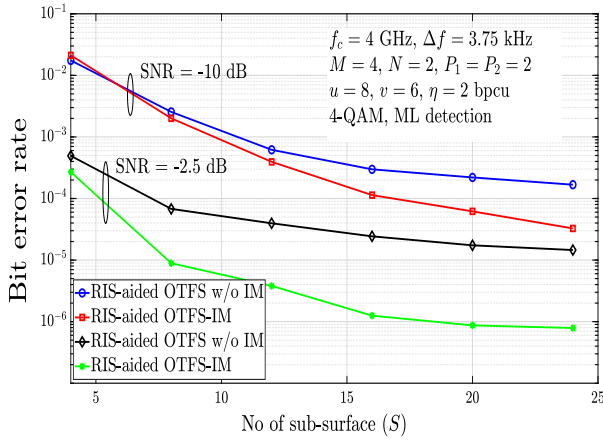


Fig. 4: Effect of number of sub-surfaces ( $S$ ) on the BER performance of RIS-aided OTFS without and with indexing.

Figure 4 shows the effect of the number of sub-surfaces  $S$  on the performance of RIS-aided OTFS without and with indexing for  $M = 4$ ,  $N = 2$ ,  $u = 8$ ,  $v = 6$ ,  $P_1 = P_2 = 2$  at SNR values of  $-10$  dB and  $-2.5$  dB. ML detection and Forbenius norm-based phase selection are considered. As the number of sub-surfaces increases, the performance of RIS-aided OTFS improves significantly, with indexing also playing a beneficial role. For example, as  $S$  varies from 4 to 24, there is a two order improvement in BER for RIS-aided OTFS with indexing, whereas there is only one order improvement in BER for RIS-aided OTFS without indexing.

In Fig. 5, we compare the BER performance of RIS-aided OTFS without and with indexing for different types of phase selection at the RIS for  $M = 4$ ,  $N = 2$ ,  $S = 16$ ,  $u = 8$ ,  $v = 6$ ,  $P_1 = P_2 = 2$ , 4-QAM, and ML detection. The performance of blind phase selection, DDRC based selection, and Frobenius norm based selection are compared. It is observed that the Frobenius norm-based phase selection has superior performance, followed by DDRC phase selection, and blind phase selection has the least performance. The superior performance of Frobenius norm-based phase selection

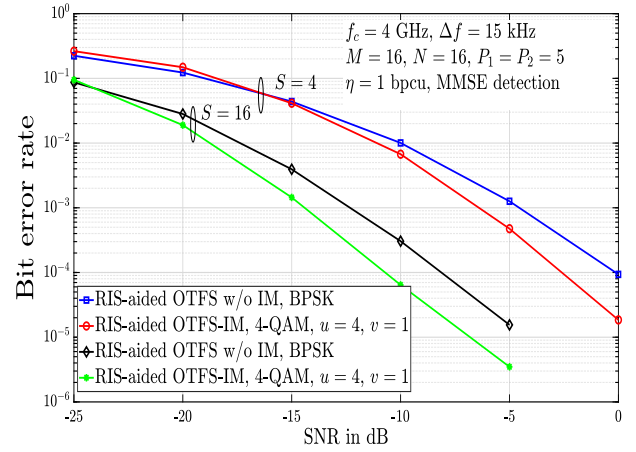


Fig. 6: BER performance of RIS-aided OTFS without and with indexing for  $M = N = 16$  and  $P_1 = P_2 = 5$ .

is due to the maximization of received SNR. Here again, the performance of RIS-aided OTFS with indexing is better than that without indexing.

*Performance for large ( $M, N$ ) values:* In Fig. 7, we present BER performance of RIS-aided OTFS without and with indexing for  $M = N = 16$ ,  $P_1 = P_2 = 5$ ,  $u = 4$ ,  $v = 1$ ,  $S = 4, 16$ , 4-QAM, Frobenius norm-based phase selection, and MMSE detection. With the above parameters, the achieved rate with indexing is 1 bpcu. We compare the performance of this system with a system without indexing with BPSK whose rate is 1 bpcu. The DD profile used is given in Table III.

It is seen that, at a BER of  $10^{-4}$ , there is an SNR gain of about 2 dB in favor of indexing compared to without indexing. Figure 7 shows the BER performance as a function of the number of sub-surfaces ( $S$ ) at SNRs of  $-10$  dB and  $-5$  dB. It can be seen that the performance of RIS-aided OTFS both without and with indexing improve as the number of sub-surfaces is increased from 4 to 24. However, there is a three order improvement in BER with indexing compared to without indexing, whereas there is only a two order improvement in BER without indexing.

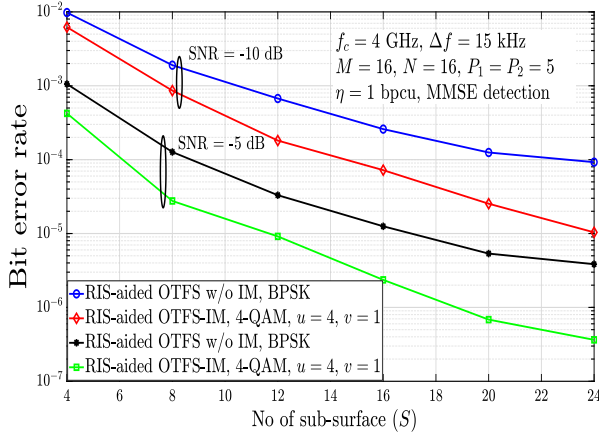


Fig. 7: Effect of number of sub-surfaces ( $S$ ) on the BER performance of RIS-aided OTFS without and with indexing for  $M = N = 16$  and  $P_1 = P_2 = 5$ .

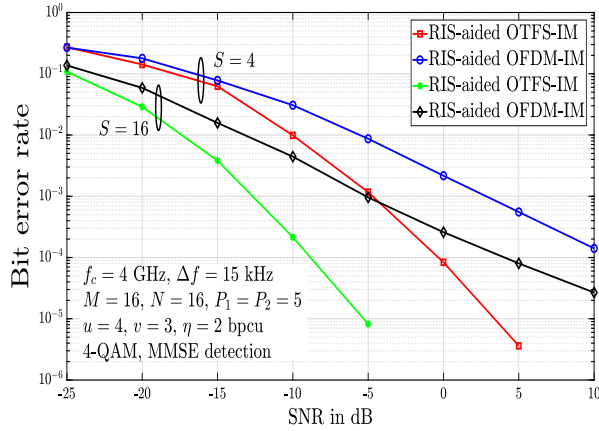


Fig. 8: BER performance comparison between RIS-aided OTFS-IM and RIS-aided OFDM-IM.

*Performance comparison between RIS-aided OTFS-IM and RIS-aided OFDM-IM:* Figure 8 shows a BER performance comparison between RIS-aided OTFS-IM with RIS-aided OFDM-IM for  $M = N = 16$ ,  $P_1 = P_2 = 5$ ,  $u = 4$ ,  $v = 3$ ,  $S = 4, 16$ , 4-QAM, Frobenius norm-based phase selection, and MMSE detection. The DD profile used is given in Table III. For RIS-aided OFDM-IM, subblock based indexing across the subcarriers given in [11] is used. From Fig. 8, we observe that the performance of RIS-aided OTFS-IM is significantly better than RIS-aided OFDM-IM. For  $S = 4$ , at a BER of  $10^{-4}$ , there is an SNR advantage of about 12 dB in favor of OTFS-IM compared to OFDM-IM. Also, as the number of sub-surfaces increases, the performance improves for both OTFS-IM and OFDM-IM schemes, with OTFS-IM achieving better performance.

## V. CONCLUSIONS

We proposed an RIS-aided OTFS scheme in which IM is carried out in the DD domain. We developed an end-to-end DD domain input-output relation for the proposed RIS-aided OTFS-IM scheme and evaluated its bit error performance. Our

simulation results showed that the performance of RIS-aided OTFS improves significantly with the proposed DD domain indexing. The results also showed that, among the phase selection schemes considered at the RIS, the Frobenius norm based phase selection offered superior performance. Also, the proposed RIS-aided OTFS-IM was shown to perform better than RIS-aided OFDM-IM. Other variants of IM with RIS-aided OTFS and indexing of sub-surfaces in the RIS are topics that can be explored for future research.

## REFERENCES

- [1] S. Hu, F. Rusek, and O. Edfors, "Beyond massive MIMO: the potential of data transmission with large intelligent surfaces," *IEEE Trans. Signal Process.*, vol. 66, no. 10, pp. 2746–2758, Mar. 2018.
- [2] Q. Wu and R. Zhang, "Intelligent reflecting surface enhanced wireless network via joint active and passive beamforming," *IEEE Trans. Wireless Commun.*, vol. 18, no. 11, pp. 5394–5409, Nov. 2019.
- [3] E. Basar, M. D. Renzo, J. de Rosny, M. Debbah, M.-S. Alouini, and R. Zhang, "Wireless communications through reconfigurable intelligent surfaces," *IEEE Access*, vol. 7, pp. 116753–116773, Aug. 2019.
- [4] B. Zheng and R. Zhang, "Intelligent reflecting surface-enhanced OFDM: channel estimation and reflection optimization," *IEEE Wireless Commun. Lett.*, vol. 9, no. 4, pp. 518–522, Apr. 2020.
- [5] R. Hadani et al., "Orthogonal time frequency space modulation," *Proc. IEEE WCNC'2017*, pp. 1–6, Mar. 2017.
- [6] P. Raviteja, K. T. Phan, Y. Hong, and E. Viterbo, "Interference cancellation and iterative detection for orthogonal time frequency space modulation," *IEEE Trans. Wireless Commun.*, vol. 17, no. 10, pp. 6501–6515, Aug. 2018.
- [7] M. K. Ramachandran and A. Chockalingam, "MIMO-OTFS in high-Doppler fading channels: signal detection and channel estimation," *Proc. IEEE GLOBECOM'2018*, pp. 206–212, Dec. 2018.
- [8] E. Basar, "Index modulation techniques for 5G wireless networks," *IEEE Commun. Mag.*, pp. 168–175, Jul. 2016.
- [9] E. Basar, M. Wen, R. Mesleh, M. Di Renzo, Y. Xiao, and H. Haas, "Index modulation techniques for next-generation wireless networks," *IEEE Access*, vol. 5, pp. 16693–16746, Sep. 2017.
- [10] B. Shamasundar, S. Jacob, S. Bhat, and A. Chockalingam, "Multidimensional index modulation in wireless communications," *IEEE Access*, vol. 6, pp. 589–604, Nov. 2018.
- [11] E. Başar, Ü. Ayoğlu, E. Panayırçı, and H. V. Poor, "Orthogonal frequency division multiplexing with index modulation," *IEEE Trans. Signal Process.*, vol. 61, no. 22, pp. 5536–5549, Nov. 2013.
- [12] Y. Liang, L. Li, P. Fan, and Y. Guan, "Doppler resilient orthogonal time-frequency space (OTFS) systems based on index modulation," *Proc. IEEE VTC'2020-Spring*, pp. 1–5, May–Jul. 2020.
- [13] J. K. Francis, R. M. Augustine, and A. Chockalingam, "Diversity and PAPR enhancement in OTFS using indexing," *Proc. IEEE VTC'2021-Spring*, pp. 1–6, Apr. 2021.
- [14] H. Zhao, D. He, Z. Kang, and H. Wang, "Orthogonal time frequency space (OTFS) with dual-mode index modulation," *IEEE Wireless Commun. Lett.*, vol. 10, no. 5, pp. 991–995, May 2021.
- [15] D. Feng, J. Zheng, B. Bai, J. Jiang, and L. Zheng, "In-phase and quadrature index modulation aided OTFS transmission," *IEEE Commun. Lett.*, vol. 26, no. 6, pp. 1318–1322, Jun. 2022.
- [16] G. Harshavardhan, V. S. Bhat, and A. Chockalingam, "RIS-aided OTFS modulation in high-Doppler channels," *Proc. IEEE PIMRC'2022*, pp. 409–415, Sep. 2022.
- [17] A. Thomas, K. Deka, S. Sharma, and N. Rajamohan, "IRS-Assisted OTFS system: design and analysis," *IEEE Trans. Veh. Tech.*, vol. 72, no. 3, pp. 3345–3358, Mar. 2023.
- [18] A. S. Bora, K. T. Phan, and Y. Hong, "IRS-assisted high mobility communications using OTFS modulation," *IEEE Wireless Commun. Lett.*, vol. 12, no. 2, pp. 376–380, Feb. 2023.